JOURNAL OF MATERIALS SCIENCE 27 (1992) 679–684

Synthesis of ultrafine single-component oxide particles by the spray-ICP technique

M. SUZUKI, M. KAGAWA, Y. SYONO, T. HIRAI
Institute for Materials Research, Tohoku University, Sendai 980, Japan

Ultrafine oxide particles were synthesized by introducing aqueous solutions of metal salts into a high-temperature r.f. inductively coupled plasma (the spray-ICP technique). The particles synthesized were spherical for ZrO_2, Y_2O_3, Sm_2O_3, La_2O_3, δ-Al_2O_3, TiO_2 (anatase), β-Bi_2O_3 and CuO, plate-like for Nd_3O_2, Cr_2O_3 and Pr_2O_3, polyhedral for PrO_2, CeO_2 and γ-Fe_2O_3, cubical for NiO, MgO, CaO, Co_3O_4 and Mn_3O_4, bar-like for SnO_2 and ZnO, and foil-like for β-PbO and MoO_3. The products of the alkaline earth group except for magnesium, were hydroxides and/or carbonates, spoiled by atmospheric H_2O and/or CO_2. The particle morphology suggests that particle growth is controlled predominantly by the gas–solid reaction occurring on the surface of nuclei condensed from the gas phase. Some of the oxides revealed a particle morphology characteristic of their crystal structures.

1. Introduction

Since Reed [1] first succeeded in generating a high-temperature r.f. inductively coupled plasma (ICP) in 1961, it has been applied for emission spectrophotometry and also for the synthesis of materials having high purity or high melting points. This is because an ICP is electrode-less, and therefore reactive gases, such as oxygen and halogens, can be treated at high temperatures. Moreover, products can be free from the contamination of electrode materials. Typical examples of material synthesis by an ICP are given for ultrafine particles of Al_2O_3–Cr_2O_3 from CrO_2Cl_2 and $AlCl_3$ vapours [2], iron from iron sponge powder [3], TaC from tantallum powder and methane [4], etc. As quoted above, in most cases, vapour or solid reactants have been used. For liquid reactants, the first report was made on the synthesis of ultrafine MgO from an aqueous $Mg(NO_3)_2$ solution [5]. This method, tentatively named the spray-ICP technique, can be applied for a wide variety of oxides, especially of the multi-component systems [6–8], because most of the metal salts are soluble in water or organic solvents and their concentration ratios can be easily adjusted to desired values when mother solutions are prepared.

The present work was aimed at extending the spray-ICP technique to the synthesis of various single-component oxide particles by describing their phase and particle morphology, to provide useful information for further application of the spray-ICP technique to multi-component oxides.

2. Experimental procedure

Mother solutions (1 M metal concentration) were prepared by dissolving nitrates of Ni, Cu, Co, Zr, La, Y, Sm, Pr, Nd, Ce, Zn, Fe, Cr, Bi, Mn, Pb, Mg, Ca, Sr and Ba, chlorides of Ti, Sn and Al (guaranteed grade) and $(NH_4)_6Mo_7O_{24}$ (guaranteed grade). They were ultrasonically atomized into fine droplets (1–2 μm in size) and were introduced (about 20 $ml\,h^{-1}$) into an argon ICP with an argon carrier gas (1.5 $l\,min^{-1}$) through a narrow-tipped quartz nozzle (1.5 mm diameter). The torch design is illustrated in Fig. 1. The ICP (40 mm diameter and 160 mm long) was generated with a three-turn r.f. coil (55 mm i.d.) and an r.f. oscillator (15 kW maximum power, 6 MHz frequency and normally run at 6 kW), and was stabilized with a helical flow of argon sheath gas (30 $l\,min^{-1}$), but no plasma gas was used. Ultrafine particles were deposited on the inside wall of a quartz tube (70 mm i.d. and 500 mm long) enclosing the tail flame of the ICP (300–500 mm long) and also with an electrostatic powder collector joined to the quartz tube. The particles were characterized by X-ray powder diffraction (XPD, CuK_α radiation with a nickel filter and a diffractometer with a graphite single-crystal monochromator) and transmission electron microscopy (JOEL JEM-2000EX). In XPD, the powders were held on a quartz plate having no background reflection peaks. Particle diameters were measured by reading about 700 particle images on transmission electron micrographs (TEM).

3. Results and discussion

In the present study, the sizes of the liquid droplets introduced into the ICP ranged from 1–2 μm. It is considered that droplets of these sizes are small enough to decompose completely to their component atoms in the ICP and the oxides are rapidly deposited from the monatomic gas phase through the condensation and solidification processes. Some of the particles deposited on the wall of the quartz tube revealed the particle growth as neck formation, caused by the heat

0022–2461/92 $03.00 + .12

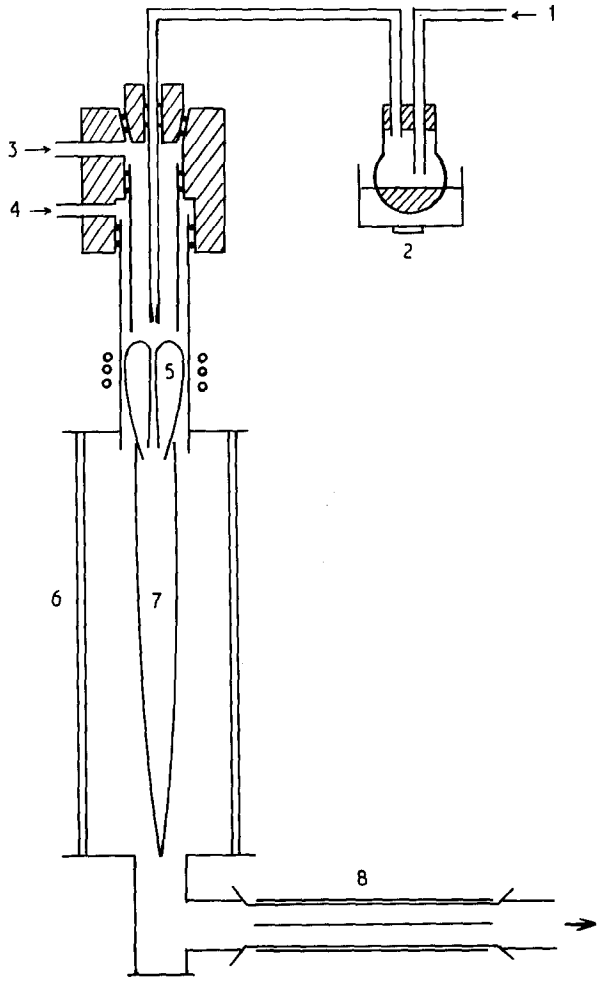

Figure 1 ICP torch. 1, Carrier gas; 2, ultrasonic atomizer; 3, plasma gas; 4, sheath gas; 5, ICP; 6, quartz tube; 7, tail flame; 8, electrostatic powder collector.

TABLE I Product, crystal system, morphology and mean particle diameter of spherical particles

Element	Product	Crystal system[a]	Morphology	Mean particle diameter (nm)
Zr	ZrO_2	t		
Y	Y_2O_3	m	A spheres	15
Sm	Sm_2O_3	m		
La	La_2O_3	h		
Nd	Nd_2O_3	h		
Cr	Cr_2O_3	h	B plates	
Pr	Pr_2O_3	h		
	PrO_2	c		
Ce	CeO_2	c	C polyhedra	
Fe	γ-Fe_2O_3	c		
Ni	NiO	c		
Mg	MgO	c		
Ca	CaO	c	D cubes	
Co	Co_3O_4	c		
Mn	Mn_3O_4	t		
Al	δ-Al_2O_3	t		
			E spheres	21
Ti	TiO_2 (anatase)	t		
Zn	ZnO	h		
			F bars	
Sn	SnO_2	t		
Bi	β-Bi_2O_3	t		26
			G spheres	
Cu	CuO	m		30
Pb	β-PbO	o		
			H foils	
Mo	MoO_3	h		

[a] t, tetragonal; m, monoclinic; h, hexagonal; c, cubic; o, orthorhombic.

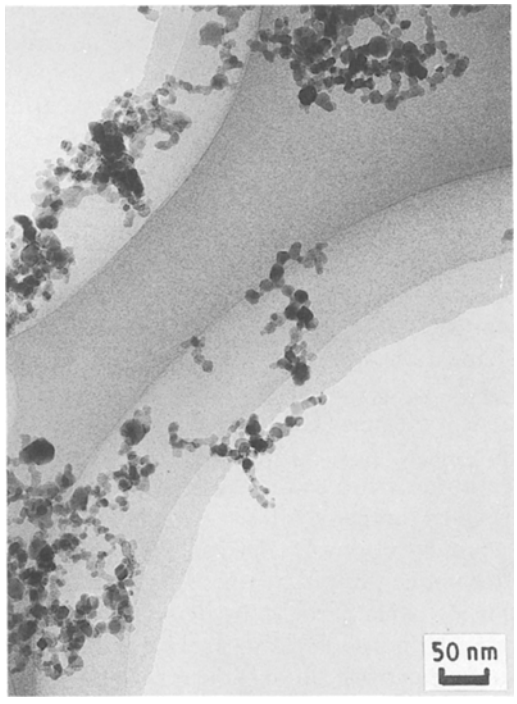

Figure 2 Transmission electron micrograph of Y_2O_3.

effect of the ICP. However, the electrostatically collected particles exhibited no trace of such particle growth, implying that they are the particles as-deposited from the ICP. The electrostatically collected particles will be described below.

Results of characterization by XPD and TEM are summarized in Tables I (oxides) and II (hydroxides and carbonates). The characteristic particle morphology of these oxides is classified into several groups, which are also given in Table I with group names from A–H. Representative TEMs are shown in Figs 2–9.

Most of the powders listed in Table I are single-phase oxides. Noteworthy is the formation of oxides having low transformation temperatures, i.e. anatase (to rutile above 645 °C), β-PbO (to α-PbO below 489 °C), γ-Fe_2O_3 (to α-Fe_2O_3 above 600 °C), β-Bi_2O_3 (to α-Bi_2O_3 below 620 °C, to δ-Bi_2O_3 above 640 °C). The irreversible transformation of rutile to anatase in particular suggests that these oxides are formed in the temperature region below their transformation temperatures. Later the process of oxide formation will be discussed in terms of the particle morphology and boiling points of oxides.

The products of the alkaline earth group except for magnesium, as listed in Table II, are hydroxides and/or carbonates. The experimental apparatus of the present study was not completely airtight, allowing atmospheric H_2O and/or CO_2, in addition to H_2O as a solvent of the mother solutions, to participate in the formation of these products. The change in product

TABLE II Products of the alkaline earth group

Element	Products
Ca	$CaO + CaCO_3 + Ca(OH)_2$
Sr	$SrCO_3$
Ba	$BaCO_3$ + unknown phase (–OH, $-CO_3$)

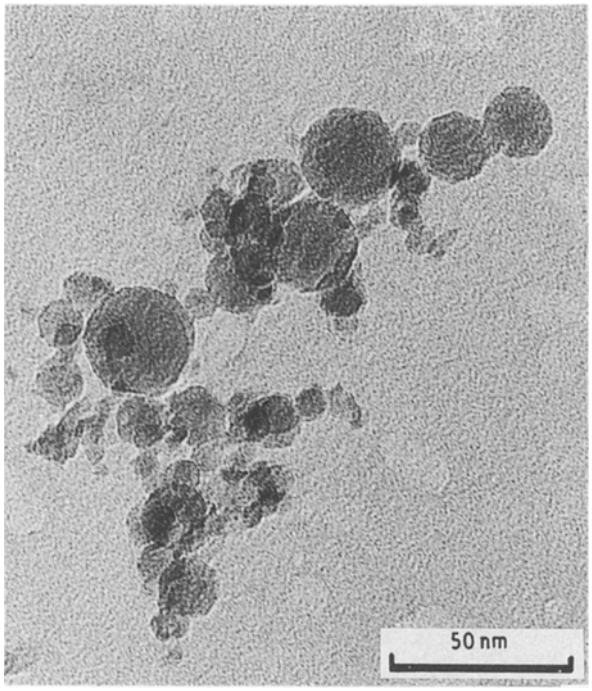

Figure 3 Transmission electron micrograph of δ-Al_2O_3.

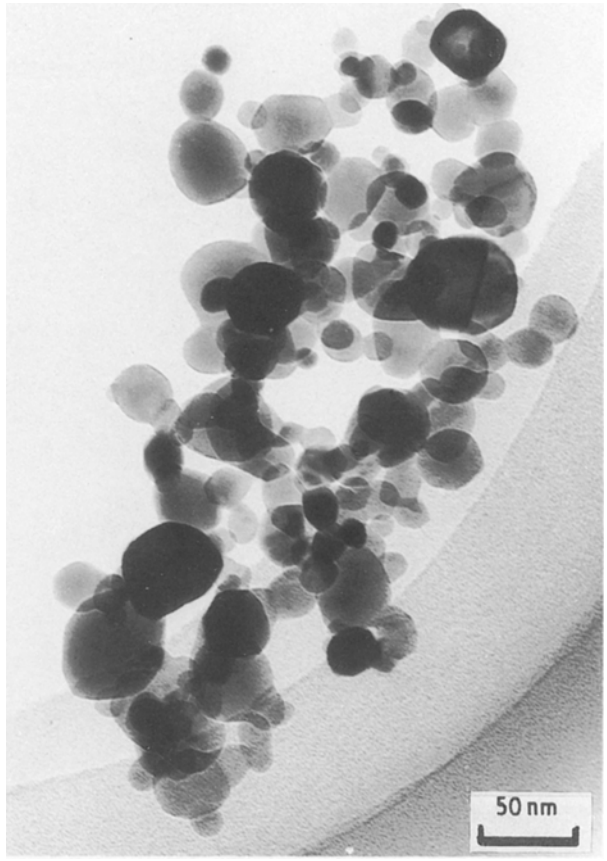

Figure 4 Transmission electron micrograph of CuO.

phase was clearly observed for the CaO, which gradually converted to $Ca(OH)_2$ and $CaCO_3$ when left in air.

The phase, particle morphology and size of the oxides synthesized by the spray-ICP technique depend on the experimental factors such as the temperature distribution in the tail flame, the velocity of evaporation of the droplets in the ICP and the vapour pressure of metals. However, they are very difficult to measure or to estimate numerically. For example, the temperature distribution in the tail flame must have the largest effect on the phase of the synthesized oxides. However, hitherto, little has been known about this effect. This is because the reaction field where the oxides are formed is very complicated to model, and because the electromagnetic noise and the strong emission from the ICP disturb the measurement of temperature with thermocouples or optical methods. In the present study, the experimental factors, e.g. feed rate of mother solutions, flow rates of carrier and sheath gases, r.f. running power, were maintained constant for all the oxide synthesis. The only different experimental factor was in the metal salts themselves, which might change the temperature distribution in the tail flame because the heat of reaction depends on the metal salts. However, the molar ratio of metal salt to water in the mother solutions was 1:55.6, which seems small enough to have no large effect on the temperature distribution in the tail flame. In the present study, therefore, all the oxides can be considered to deposit under the same conditions. Therefore, the particle morphology reflects the reaction processes cited below and some intrinsic properties of each oxide.

The first precursors formed by the condensation from the monatomic gas phase are liquid. They coalesce with each other into large droplets and then solidify (coalescence growth). This process, therefore, tends to bring about the formation of spherical particles. In another case, the liquid precursors solidify to crystals before the coalescence growth takes place, and the crystals grow large by the gas–solid reaction occurring on the crystal surface (gas–solid reaction). In view of these two types of reaction processes, qualitatively the temperature of condensation can be related to the boiling point of oxides (b.p.). The solidification process of the coalescence growth and the crystal growth process of the gas–solid reaction determine the particle morphology and size.

The particle morphology, and temperature differences between boiling and melting points of the oxides concerned (expressed by bars [9–14]) are illustrated in Fig. 10.

In the present study, the gas–solid reaction is more likely to participate in the particle growth. Except for the case of spherical particles of Groups A, E and G, all the particles have a clear particle morphology as large hexagonal plates (Group B), polyhedra (C), bars (F) and thin foils (H). The formation of these particles can be explained in terms of the gas–solid reaction,

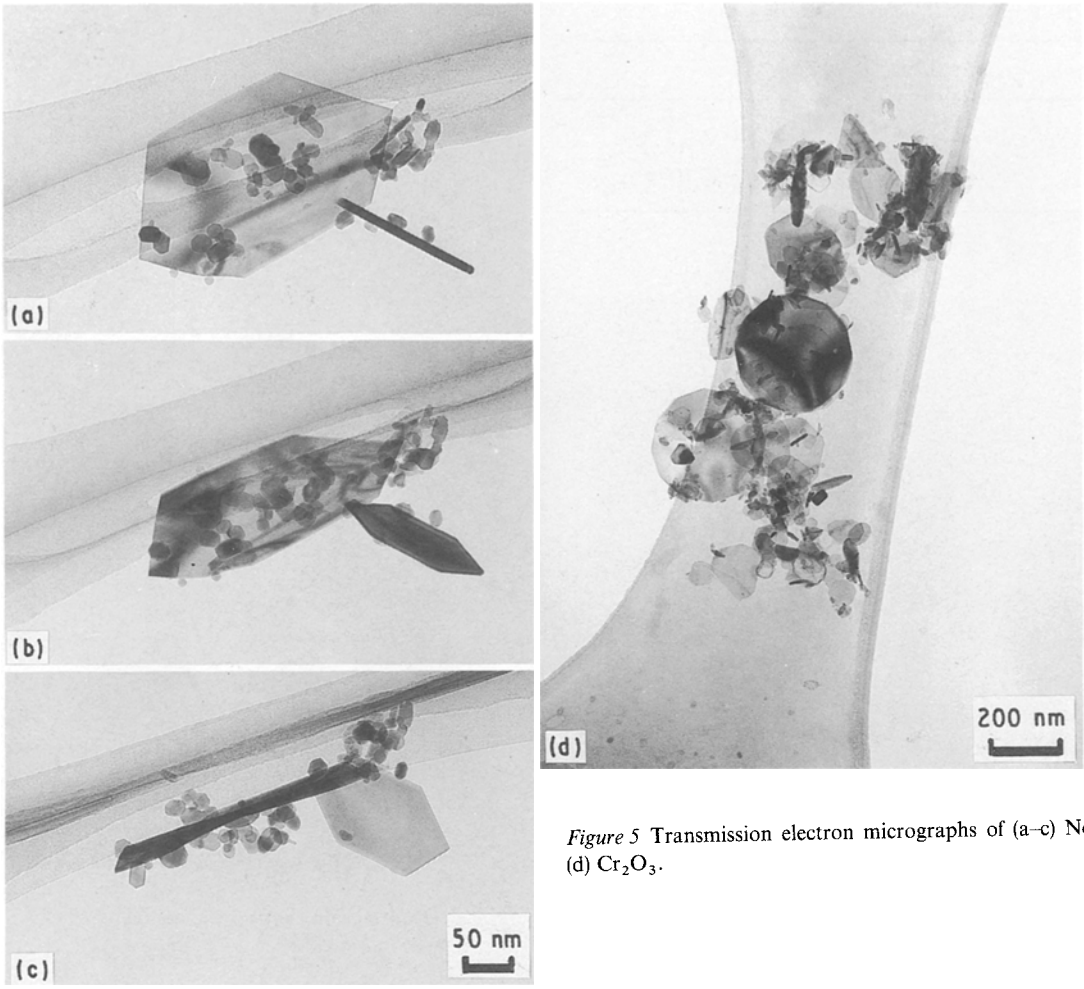

Figure 5 Transmission electron micrographs of (a–c) Nd_2O_3 and (d) Cr_2O_3.

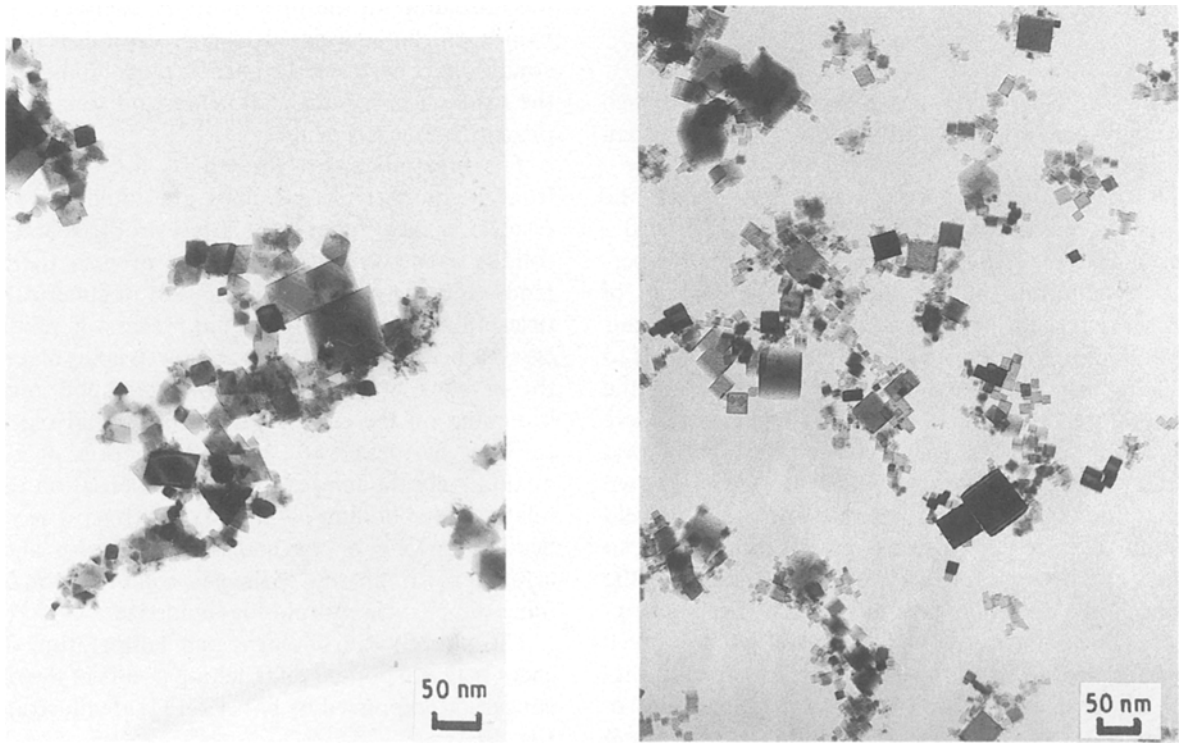

Figure 6 Transmission electron micrograph of CeO_2.

Figure 7 Transmission electron micrograph of NiO.

and not of the coalescence growth. It seems reasonable to consider that the spherical particles (A, E and G) are also formed by the gas–solid reaction, because in Fig. 10 these groups locate in the series of Groups B, C, D and F which are related to the gas–solid reaction. Gani and McPherson [15] synthesized particles of the Ti–Al–O system by introducing gaseous Al_2Br_6 and $TiCl_4$ into the tail flame of an ICP at much higher

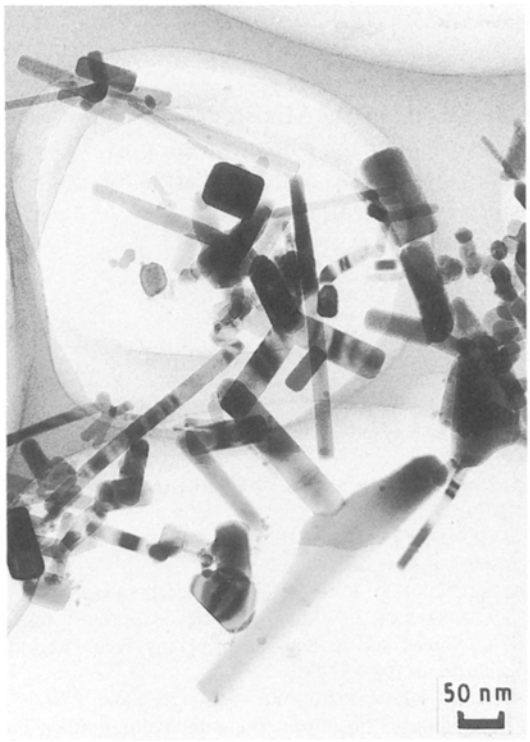

Figure 8 Transmission electron micrograph of ZnO.

Figure 9 Transmission electron micrograph of β-PbO.

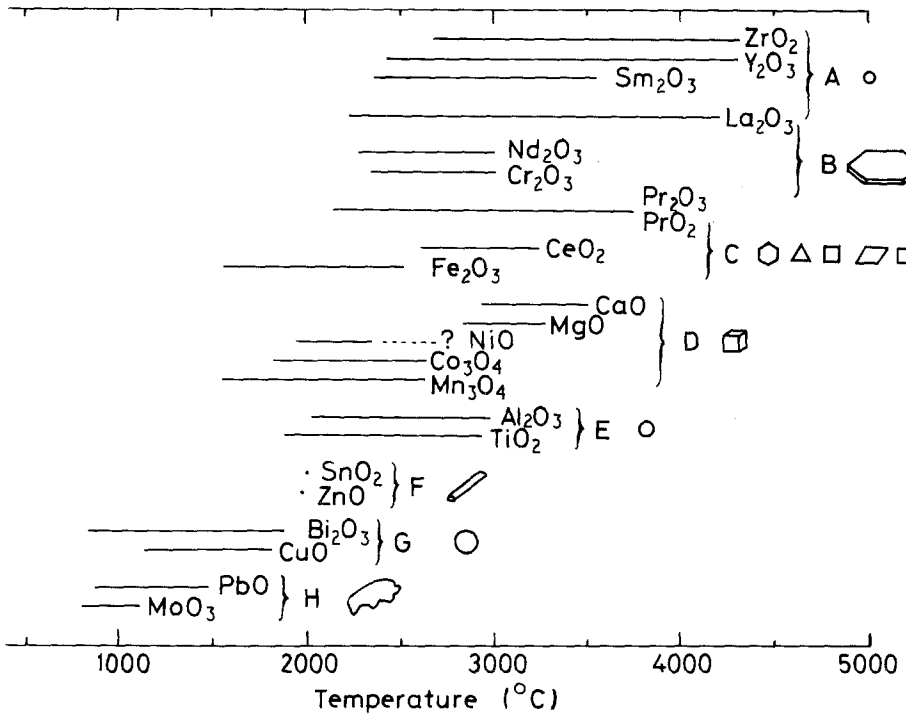

Figure 10 Particle morphology and temperature differences between boiling and melting points of oxides [9–14].

powder production rates than those of the present study. They reported that the formation process of these oxides is controlled by the coalescence growth and the particle size is determined by the difference between condensation and solidification temperatures. The smallest mean diameter for the TiO_2 is about 38 nm (log normal, at a powder production rate of 1 g min^{-1}), while those of the present study fell around 20 nm (at 27 mg min^{-1}, calculated from the feed rate and concentration of the mother solution). This difference is twice in particle diameter, but eight times in volume. The participation of the gas–solid reaction in the formation of spherical particles in the present study can be attributed to the low powder production rate, that is, the low reactant vapour pressure in the ICP.

The particles of La_2O_3 were spherical, but a very few anomalously large hexagonal plates were formed together. Most particles of Nd_2O_3 and Cr_2O_3 were plates, as proved by TEM taken at different angles for a certain Nd_2O_3 particle (Fig. 5). The plate-like Cr_2O_3 was also formed when synthesized by the injection of gaseous CrO_2Cl_2 [2]. The powders of the Pr–O system exhibited two phases, i.e. Pr_2O_3 and PrO_2. TEM clarified that they were composed of plates and polyhedra. The former were identified as Pr_2O_3 and the latter as PrO_2. As a whole, the particle morphology reflects the crystal structure of oxides. The oxides of the A-rare-earth type (hexagonal: La_2O_3, Nd_2O_3, Pr_2O_3) and of the corundum type (hexagonal: Cr_2O_3) tend to form plates. Those of the cubic fluorite type (CeO_2, PrO_2) and of the NaCl type (CaO, MgO, NiO) grow to polyhedra and cubes, respectively. However, further investigation is required to establish this criterion.

The mean particle diameter of the sphere group (A, E, G) increases as b.p. decreases, indicating that oxides of high b.p. cannot grow larger than those of low b.p. This suggests that the former are condensed in the higher temperature region and quenched more rapidly than the latter.

The difference in b.p. affects the particle morphology in some cases. La_2O_3 and Y_2O_3, having almost the same high b.p., produced spheres. However, the former contained plates as a very minor product. Nd_2O_3 of much lower b.p. was composed of mainly plates and a small amount of cubes. This difference in number of plates compared to spheres or cubes can be explained in terms of the difference in b.p. That is, La_2O_3 tends to deposit faster without forming the plates than Nd_2O_3, because of its high b.p.

As mentioned before, Fe_2O_3, TiO_2, PbO and Bi_2O_3 are formed in the much lower temperature region than their b.p.

In conclusion, under the conditions of the present study, the gas–solid reaction predominates the particle growth, which is attributed to the low reactant vapour pressure in the ICP. Each oxide tends to reveal the particle morphology characteristic of its crystal structure. The particle morphology and size also depend on the b.p. of the oxides, because it is a factor controlling the solidification process. These results should be taken into account when the spray-ICP technique is extended to the multi-component oxide systems.

Acknowledgements

The authors thank the Ministry of Education, Science, and Culture, Japan, for financial support, T. Nihei for glass blowing work, and S. Morita for conducting transmission electron microscopy.

References

1. T. B. REED, *J. Appl. Phys.* **32** (1961) 821.
2. T. I. BARRY, R. K. BAYLISS and L. A. LAY, *J. Mater. Sci.* **3** (1968) 229.
3. T. YOSHIDA and K. AKASHI, *Trans. Jpn Inst. Metals* **22** (1981) 371.
4. J. CANTELOUP and A. MOCELLIN, *J. Mater. Sci.* **11** (1976) 2352.
5. M. KAGAWA, M. KIKUCHI, R. OHNO and T. NAGAE, *J. Amer. Ceram. Soc.* **64** (1981) C7.
6. M. SUZUKI, M. KAGAWA, T. B. WILLIAMS, Y. SYONO and T. HIRAI, in "Materials Science Forum", edited by C. C. Sorrell and B. Ben-Nissan (Trans Tech Publications, Switzerland, 1988) p. 791.
7. M. SUZUKI, M. KAGAWA, Y. SYONO and T. HIRAI, *in* "Proceedings of the 9th International Symposium on Plasma Chemistry", Pugnochiuso, Italy, 1989, edited by R. d'Agostino, p. 898.
8. *Idem, J. Crystal Growth* **99** (1990) 611.
9. G. V. SAMSONOV, in "The Oxide Handbook" (IFI/Plenum, New York, 1973).
10. I. BARIN, in "Thermochemical Data of Pure Substances" (VCH, Weinheim, 1989).
11. D. R. STULL and H. PROPHET, in "JANAF Thermochemical Tables", 2nd Edn (National Bureau of Standards, Washington, DC, 1971).
12. M. W. CHASE, *et al.*, in "JANAF Thermochemical Tables", 3rd Edn (National Bureau of Standards, Washington, DC, 1985).
13. O. KUBASCHEWSKI and C. B. ALOCK, in "Metallurgical Thermochemistry", 5th Edn (Pergamon Press, Oxford, 1979).
14. R. E. KRJIJANOFSKI and A. IU. SHTERN, in "Thermophysical Properties of Metal Oxides" (Energiia Press, Leningrad, 1973).
15. M. S. J. GANI and R. McPHERSON, *J. Mater. Sci.* **15** (1980) 1915.

Received 4 October 1990
and accepted 20 March 1991